

Effects of nuclear deformation and neutron transfer in capture processes, and fusion hindrance at deep sub-barrier energies

V. V. Sargsyan,^{1,2} G. G. Adamian,¹ N. V. Antonenko,¹ W. Scheid,³ and H. Q. Zhang⁴

¹*Joint Institute for Nuclear Research, 141980 Dubna, Russia*

²*International Center for Advanced Studies, Yerevan State University, 0025 Yerevan, Armenia*

³*Institut für Theoretische Physik der Justus-Liebig-Universität, D-35392 Giessen, Germany*

⁴*China Institute of Atomic Energy, 102413 Beijing, China*

(Received 7 November 2011; published 22 December 2011)

The roles of nuclear deformation and neutron transfer in sub-barrier capture process are studied within the quantum diffusion approach. The change of the deformations of colliding nuclei with neutron exchange can crucially influence the sub-barrier fusion. The comparison of the calculated capture cross section and the measured fusion cross section in various reactions at extreme sub-barrier energies gives us information about the quasifission.

DOI: [10.1103/PhysRevC.84.064614](https://doi.org/10.1103/PhysRevC.84.064614)

PACS number(s): 25.70.Jj, 24.10.-i, 24.60.-k

I. INTRODUCTION

The nuclear deformation and neutron-transfer process have been identified as playing a major role in the magnitude of the sub-barrier capture and fusion cross sections [1–3]. There are several experimental evidences which confirm the importance of nuclear deformation on the capture and fusion. The influence of nuclear deformation is straightforward. If the target nucleus is prolate in the ground state, the Coulomb field on its tips is lower than on its sides, that then increases the capture or fusion probability at energies below the barrier corresponding to the spherical nuclei. The role of neutron transfer reactions is less clear. A correlation between the overall transfer strength and fusion enhancement was firstly noticed in Ref. [4]. The importance of neutron transfer with positive Q values on nuclear fusion (capture) originates from the fact that neutrons are insensitive to the Coulomb barrier and therefore they can start being transferred at larger separations before the projectile is captured by target nucleus [5]. Therefore, it is generally thought that the sub-barrier fusion cross section will increase [6–9] because of the neutron transfer. As suggested in Ref. [10], the enhancements in fusion yields may be from the transfer of a neutron pair with a positive Q value. However, as shown recently in Ref. [11], the two-neutron transfer channel with large positive Q value weakly influences the fusion (capture) cross section in the $^{60}\text{Ni}+^{100}\text{Mo}$ reaction at sub-barrier energies. So, from the present data an unambiguous signature of the role of the neutron transfer channel could not be inferred.

The experiments with various medium-light and heavy systems have shown that the experimental slopes of the complete fusion excitation function keep increasing at low sub-barrier energies and may become much larger than the predictions of standard coupled-channel calculations. This was identified as the fusion hindrance [12]. More experimental and theoretical studies of sub-barrier fusion hindrance are needed to improve our understanding of its physical reason, which may be especially important in astrophysical fusion reactions [13].

It is worth remembering that the first evidences of hindrance for compound nucleus formation in the reactions with massive nuclei ($Z_1 \times Z_2 > 1600$) at energies near the Coulomb barrier

were observed at GSI already a long time ago [14]. The theoretical investigations showed that the probability of complete fusion depends on the competition between the complete fusion and quasifission after the capture stage [15–17]. As known, this competition can strongly reduce the value of the fusion cross section and, respectively, the value of the evaporation residue cross section in the reactions producing superheavy nuclei. Although the quasifission was originally ascribed to the reactions with massive nuclei, it is the general phenomenon which is related to the binary decay of nuclear system after the capture, but before the compound nucleus formation which could exist at angular momenta treated. The mass and angular distributions of the quasifission products depend on the entrance channel and bombarding energy [15]. Because the capture cross section is the sum of the fusion and quasifission cross sections, from the comparison of calculated capture cross sections and measured fusion cross sections one can extract the hindrance factor and show a role of the quasifission channel in the reactions with various medium-mass and heavy nuclei at extreme sub-barrier energies.

In the present paper the quantum diffusion approach [18,19] is applied to study the fusion hindrance and the roles of nuclear deformation and neutron transfer in sub-barrier capture process. With this approach many heavy-ion capture reactions at energies above and well below the Coulomb barrier have been successfully described [18–21]. Because the details of our theoretical treatment were already published in Refs. [18–22], the model will be shortly described in Sec. II. In Sec. III, a reduction procedure will be proposed to eliminate the influence of the nucleus-nucleus potential on the fusion (capture) cross section. The calculated results will be presented in Secs. IV and V.

II. MODEL

In the quantum diffusion approach the collisions of nuclei are treated in terms of a single collective variable: the relative distance between the colliding nuclei. The nuclear deformation effects are taken into consideration through the dependence of the nucleus-nucleus potential on the deformations and orientations of colliding nuclei. Our approach takes into

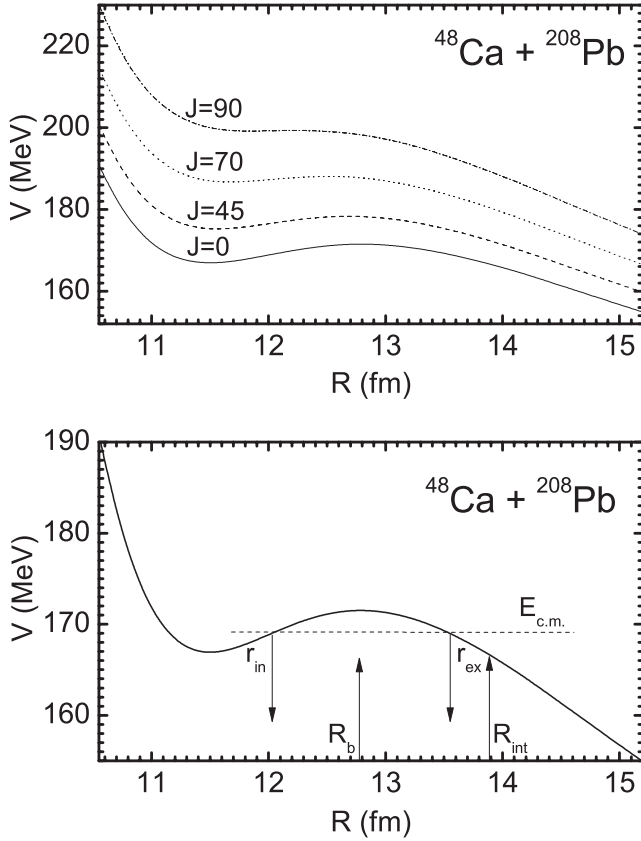


FIG. 1. (Upper part) The nucleus-nucleus potentials calculated at $J=0$ (solid curve), 45 (dashed curve), 70 (dotted curve), and 90 (dash-dotted curve) for the $^{48}\text{Ca}+^{208}\text{Pb}$ reaction. The interacting nuclei are assumed to be spherical in the calculation. (Lower part) The position R_b of the Coulomb barrier, radius of interaction R_{int} , and external r_{ex} and internal r_{in} turning points for some values of bombarding energy $E_{\text{c.m.}}$ are indicated at the nucleus-nucleus potential for the same reaction at $J=0$.

consideration the fluctuation and dissipation effects in collisions of heavy ions which model the coupling with various channels (for example, coupling of the relative motion with low-lying collective modes such as dynamical quadrupole and octupole modes of target and projectile [23]). We have to mention that many quantum-mechanical and non-Markovian effects accompanying the passage through the potential barrier are taken into consideration in our formalism [18–22,24,25]. The details of used formalism are presented in our previous articles [18,19]. One should stress that the diffusion model which is including the quantum statistical effects was also proposed in Refs. [26–28].

The capture cross section is a sum of partial capture cross sections [18,19],

$$\begin{aligned} \sigma_{\text{cap}}(E_{\text{c.m.}}) &= \sum_J \sigma_{\text{cap}}(E_{\text{c.m.}}, J) \\ &= \pi \lambda^2 \sum_J (2J+1) \int_0^{\pi/2} d\theta_1 \sin(\theta_1) \\ &\quad \times \int_0^{\pi/2} d\theta_2 \sin(\theta_2) P_{\text{cap}}(E_{\text{c.m.}}, J, \theta_1, \theta_2), \end{aligned} \quad (1)$$

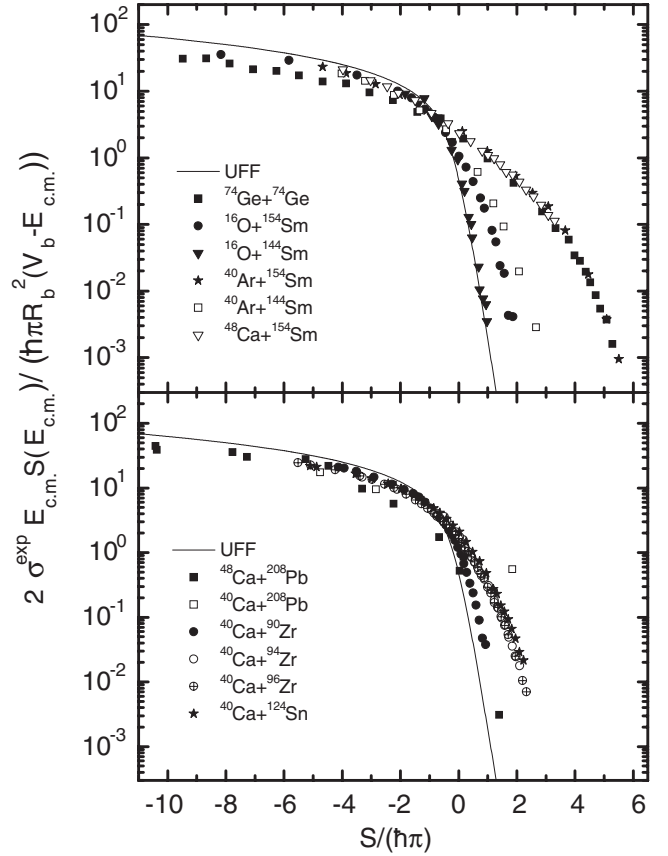


FIG. 2. Comparison of modified UFF F_0 with the experimental values of $\frac{2E_{\text{c.m.}}S(E_{\text{c.m.}})}{h\pi R_b^2(V_b - E_{\text{c.m.}})} \sigma^{\text{exp}}$ for the indicated reactions. The experimental data for σ^{exp} are from Refs. [32–39].

where $\lambda^2 = \hbar^2/(2\mu E_{\text{c.m.}})$ is the reduced de Broglie wavelength, $\mu = m_0 A_1 A_2 / (A_1 + A_2)$ is the reduced mass (m_0 is the nucleon mass), and the summation is over the possible values of angular momentum J at a given bombarding energy $E_{\text{c.m.}}$. Knowing the potential of the interacting nuclei for each orientation, one can obtain the partial capture probability P_{cap} which is defined by the passing probability of the potential barrier in the relative distance R coordinate at a given J . The value of P_{cap} is obtained by integrating the propagator G from the initial state (R_0, P_0) at time $t=0$ to the final state (R, P) at time t (P is a momentum):

$$\begin{aligned} P_{\text{cap}} &= \lim_{t \rightarrow \infty} \int_{-\infty}^{r_{\text{in}}} dR \int_{-\infty}^{\infty} dP G(R, P, t | R_0, P_0, 0) \\ &= \lim_{t \rightarrow \infty} \frac{1}{2} \text{erfc} \left[\frac{-r_{\text{in}} + \overline{R(t)}}{\sqrt{\Sigma_{RR}(t)}} \right]. \end{aligned} \quad (2)$$

The second line in Eq. (2) is obtained by using the propagator $G = \pi^{-1} |\det \Sigma^{-1}|^{1/2} \exp(-\mathbf{q}^T \Sigma^{-1} \mathbf{q})$ ($\mathbf{q}^T = [q_R, q_P]$, $q_R(t) = R - \overline{R(t)}$, $q_P(t) = P - \overline{P(t)}$, $\overline{R(t=0)} = R_0$, $\overline{P(t=0)} = P_0$, $\Sigma_{kk'}(t) = 2q_k(t)q_{k'}(t)$, $\Sigma_{kk'}(t=0) = 0$, $k, k' = R, P$) calculated in Ref. [29] for an inverted oscillator which approximates the nucleus-nucleus potential V in the variable R . The frequency ω of this oscillator with an internal turning point r_{in} is defined from the condition of

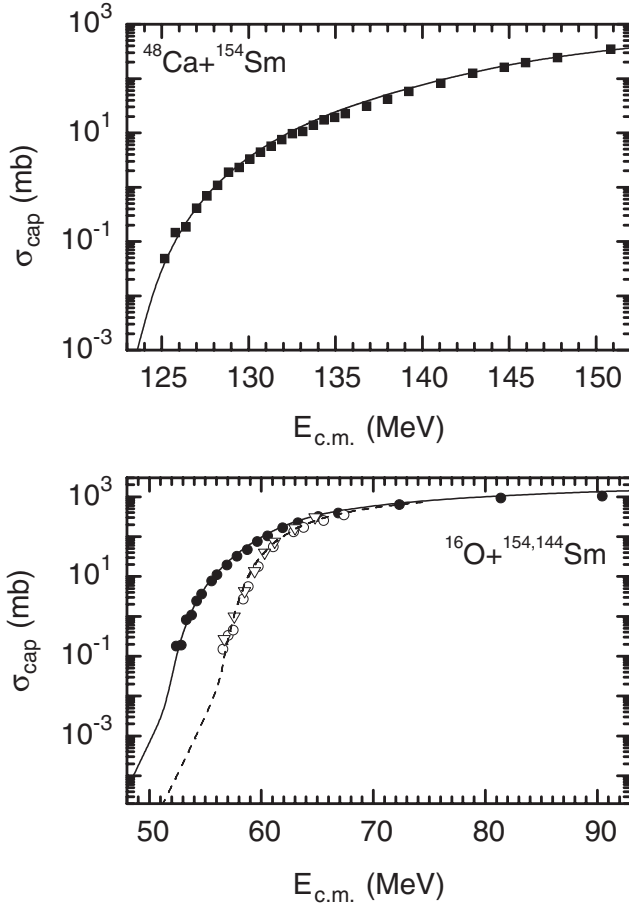


FIG. 3. The calculated capture cross sections versus $E_{c.m.}$ for the indicated reactions $^{16}\text{O}+^{48}\text{Ca}+^{154}\text{Sm}$ (solid lines), and $^{16}\text{O}+^{144}\text{Sm}$ (dashed line). The experimental data (symbols) are from Refs. [32–34]. The following quadrupole deformation parameters are used: $\beta_2(^{154}\text{Sm})=0.341$ [40], $\beta_2(^{144}\text{Sm})=0.05$, and $\beta_2(^{16}\text{O})=\beta_2(^{48}\text{Ca})=0$.

equality of the classical actions of approximated and realistic potential barriers of the same height at given J (see Fig. 1). It should be noted that the passage through the Coulomb barrier approximated by a parabola was previously studied in Refs. [24–28]. This approximation is well justified for the reactions and energy range, which are here considered. Finally, one can find the expression for the capture probability:

$$P_{\text{cap}} = \frac{1}{2} \text{erfc} \left[\left(\frac{\pi s_1 (\gamma - s_1)}{2 \hbar \mu (\omega_0^2 - s_1^2)} \right)^{1/2} \frac{\mu \omega_0^2 R_0 / s_1 + P_0}{[\gamma \ln(\gamma / s_1)]^{1/2}} \right], \quad (3)$$

where γ is the internal-excitation width, $\omega_0^2 = \omega^2 \{1 - \hbar \tilde{\lambda} \gamma / [\mu (s_1 + \gamma)(s_2 + \gamma)]\}$ is the renormalized frequency in the Markovian limit, the value of $\tilde{\lambda}$ is related to the strength of linear coupling in coordinates between collective and internal subsystems. The s_i are the real roots ($s_1 \geq 0 > s_2 \geq s_3$) of the following equation:

$$(s + \gamma)(s^2 - \omega_0^2) + \hbar \tilde{\lambda} \gamma s / \mu = 0. \quad (4)$$

The details of the used formalism are presented in Refs. [18,19]. We have to mention that most of the quantum-

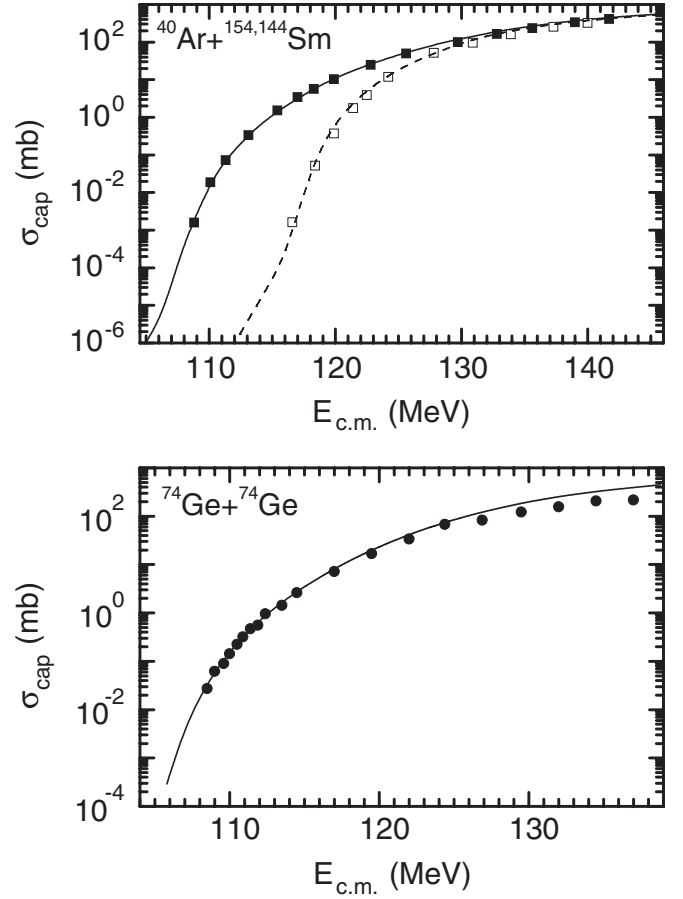


FIG. 4. The same as Fig. 3 for the indicated reactions $^{74}\text{Ge}+^{74}\text{Ge}$, $^{40}\text{Ar}+^{154}\text{Sm}$ (solid lines), and $^{40}\text{Ar}+^{144}\text{Sm}$ (dashed line). The experimental data (symbols) are from Refs. [35, 36]. The following quadrupole deformation parameters are used: $\beta_2(^{40}\text{Ar})=0.25$ [40], $\beta_2(^{74}\text{Ge})=0.2825$ [40], $\beta_2(^{154}\text{Sm})=0.341$ [40], and $\beta_2(^{144}\text{Sm})=0.05$.

mechanical, dissipative effects and non-Markovian effects accompanying the passage through the potential barrier are taken into consideration in our formalism [18,19,24]. For example, the non-Markovian effects appear in the calculations through the internal-excitation width γ .

As shown in Refs. [18,19], the nuclear forces start to play a role at $R_{\text{int}} = R_b + 1.1$ fm where the nucleon density of colliding nuclei approximately reaches 10% of the saturation density. If the value of r_{ex} corresponding to the external turning point is larger than the interaction radius R_{int} , we take $R_0 = r_{\text{ex}}$ and $P_0 = 0$ in Eq. (3) (see Fig. 1). For $r_{\text{ex}} < R_{\text{int}}$, it is naturally to start our treatment with $R_0 = R_{\text{int}}$ and P_0 defined by the kinetic energy at $R = R_0$. In this case the friction hinders the classical motion to proceed toward smaller values of R . If $P_0 = 0$ at $R_0 > R_{\text{int}}$, the friction almost does not play a role in the transition through the barrier. Thus, two regimes of interaction at sub-barrier energies differ by the action of the nuclear forces and the role of friction at $R = r_{\text{ex}}$.

In addition to the parameters related to the nucleus-nucleus potential, two parameters $\hbar \gamma = 15$ MeV and the friction coefficient $\hbar \lambda = -\hbar (s_1 + s_2) = 2$ MeV are used for calculating

the capture probability in reactions with deformed actinides. The value of $\tilde{\lambda}$ is set to obtain this value of $\hbar\lambda$. The most realistic friction coefficients in the range of $\hbar\lambda \approx 1 - 2$ MeV are suggested from the study of deep inelastic and fusion reactions [30]. These values are close to those calculated within the mean-field approach [31]. All calculated results presented are obtained with the same set of parameters and are rather insensitive to a reasonable variation of them [18,19,24,25]. All parameters of the model are set as in Ref. [18]. All calculated results are obtained with the same set of parameters and are rather insensitive to the reasonable variation of them [18,19]. The heights of the calculated Coulomb barriers $V_b = V(R_b)$ (R_b is the position of the Coulomb barrier) are adjusted to the experimental data for the fusion or capture cross sections. To calculate the nucleus-nucleus interaction potential $V(R)$, we use the procedure presented in Refs. [18,19]. For the nuclear part of the nucleus-nucleus potential, the double-folding formalism with the Skyrme-type density-dependent effective nucleon-nucleon interaction is used.

III. UNIVERSAL FUSION FUNCTION

To analyze the experimental data on fusion cross section, it is useful to use the so-called universal fusion function (UFF) F_0

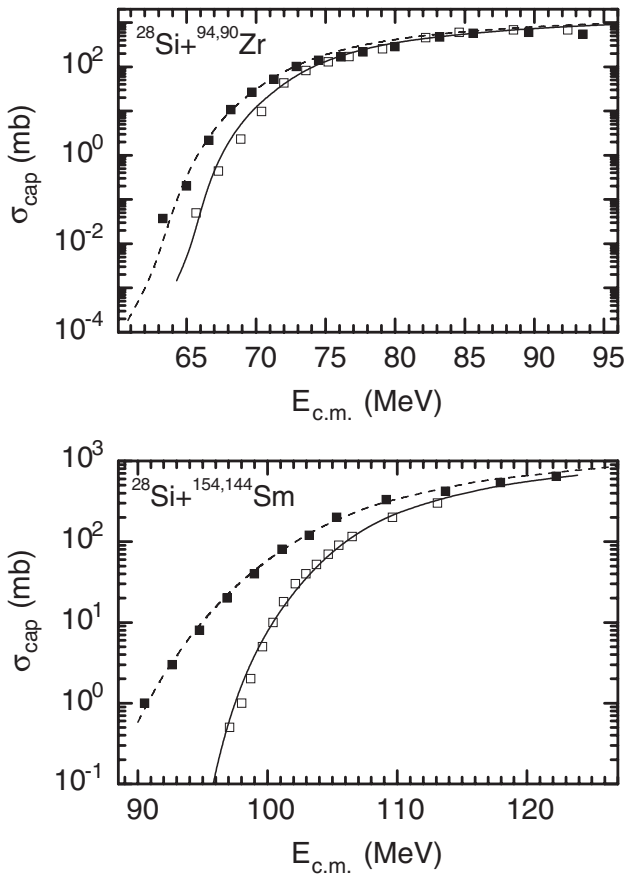


FIG. 5. The same as Fig. 3, for the indicated reactions $^{28}\text{Si}+^{94}\text{Zr}, ^{154}\text{Sm}$ (solid lines), and $^{28}\text{Si}+^{90}\text{Zr}, ^{144}\text{Sm}$ (dashed lines). The experimental data (symbols) are from Refs. [42–44]. The following quadrupole deformation parameters are used: $\beta_2(^{154}\text{Sm}) = 0.341$ [40], $\beta_2(^{144}\text{Sm}) = 0.05$, and $\beta_2(^{28}\text{Si}) = 0.3$.

[2]. The advantages of UFF appear clearly when one wants to compare fusion cross sections for systems with quite different Coulomb barrier heights and positions. In the reactions where the capture and fusion cross sections coincide, the comparison of experimental cross sections with the UFF allows us to make conclusions about the role of deformation of colliding nuclei and the nucleon transfer between interacting nuclei in the capture cross section because the UFF (the consequence of the Wong's formula) does not contain these effects. In Ref. [2] a reduction procedure was proposed to eliminate the influence of the nucleus-nucleus potential on the fusion cross section. It consists of the following transformations:

$$E_{c.m.} \rightarrow x = \frac{E_{c.m.} - V_b}{\hbar\omega},$$

$$\sigma^{\text{exp}} \rightarrow F(x) = \frac{2E_{c.m.}}{\hbar\omega R_b^2} \sigma^{\text{exp}}.$$

The frequency $\omega = \sqrt{V''(R_b)/\mu}$ is related with the second derivative $V''(R_b)$ of the total nucleus-nucleus potential $V(R)$ (the Coulomb + nuclear parts) at the barrier radius R_b and the reduced mass parameter μ . With these replacements one can

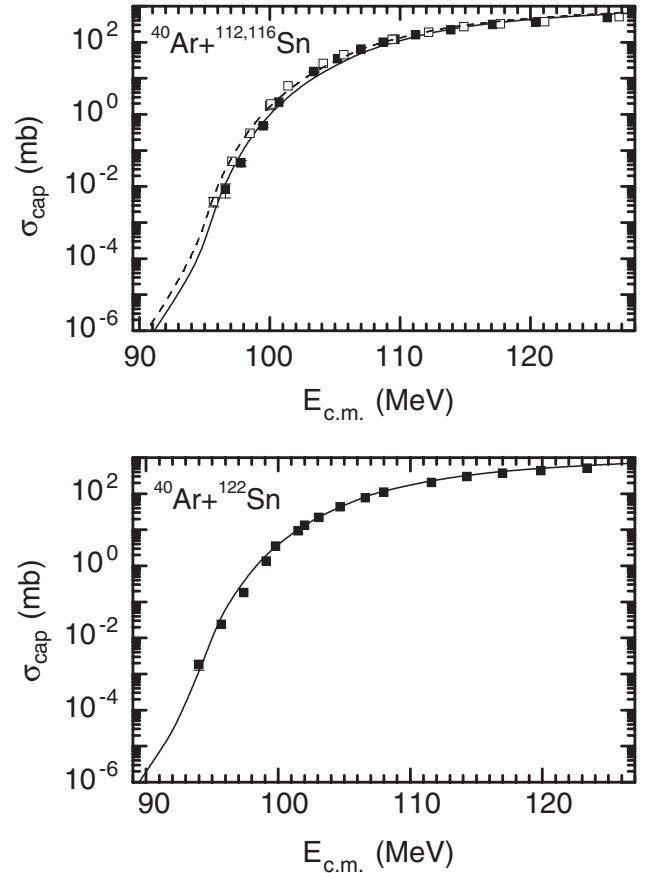


FIG. 6. The same as Fig. 3, for the indicated reactions $^{40}\text{Ar}+^{112,122}\text{Sn}$ (solid lines), and $^{40}\text{Ar}+^{116}\text{Sn}$ (dashed line). The experimental data (symbols) are from Ref. [36]. The following quadrupole deformation parameters are used: $\beta_2(^{112}\text{Sn}) = 0.1227$ [40], $\beta_2(^{116}\text{Sn}) = 0.1118$ [40], $\beta_2(^{122}\text{Sn}) = 0.1036$ [40], and $\beta_2(^{40}\text{Ar}) = 0.25$ [40].

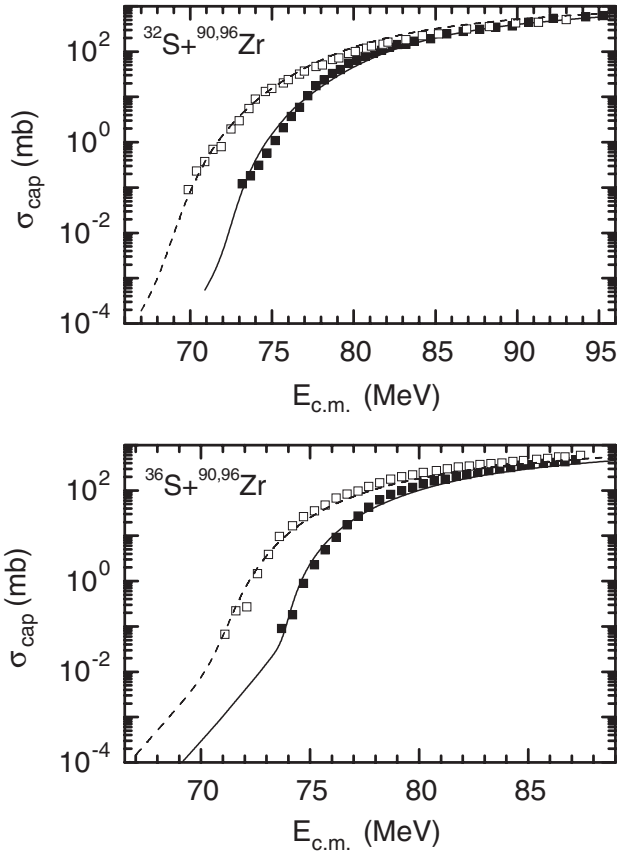


FIG. 7. The same as Fig. 3, for the indicated reactions $^{36,32}\text{S}+^{90}\text{Zr}$ (solid lines), and $^{36,32}\text{S}+^{96}\text{Zr}$ (dashed lines). The experimental data (symbols) are from Refs. [45,46]. The following quadrupole deformation parameters are used: $\beta_2(^{32}\text{S}) = 0.312$ [40], $\beta_2(^{34}\text{S}) = 0.252$ [40], $\beta_2(^{96}\text{Zr}) = 0.08$, and $\beta_2(^{90}\text{Zr}) = 0$.

compare the experimental data for different reactions. After these transformations, the reduced calculated fusion cross section takes the simple form,

$$F_0 = \ln[1 + \exp(2\pi x)].$$

To take into consideration the deviation of the real potential from the inverted oscillator, we modify the reduction procedure as follows:

$$E_{c.m.} \rightarrow x = S/(\hbar\pi),$$

$$\sigma^{\text{exp}} \rightarrow F(x) = \frac{2SE_{c.m.}}{\hbar\pi R_b^2(V_b - E_{c.m.})} \sigma^{\text{exp}}.$$

In this case,

$$F_0 = \ln[1 + \exp(-2S/\hbar)],$$

where $S(E_{c.m.})$ is the classical action. At energies above the Coulomb barrier, we have $S = \pi(V_b - E_{c.m.})/\omega$.

IV. RESULTS OF CALCULATIONS

A. Effect of quadrupole deformation

In Fig. 2 (upper part), one can see the comparisons of dependencies F and F_0 on $S/(\hbar\pi)$ for some reactions

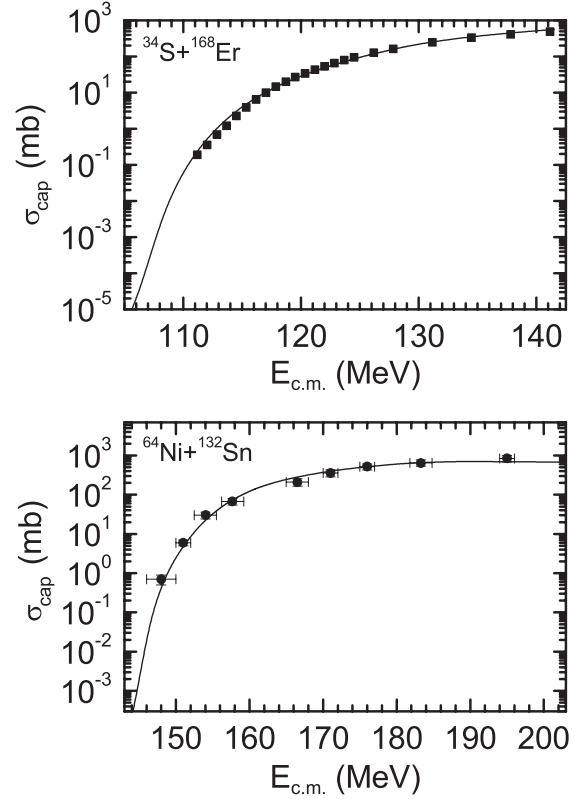


FIG. 8. The same as Fig. 3, for the indicated reactions $^{34}\text{S}+^{168}\text{Er}$ and $^{64}\text{Ni}+^{132}\text{Sn}$. The experimental data (symbols) are from Refs. [47,48]. The following quadrupole deformation parameters are used: $\beta_2(^{168}\text{Er}) = 0.3381$ [40], $\beta_2(^{66}\text{Ni}) = 0.158$ [40], $\beta_2(^{130}\text{Sn}) = 0$, and $\beta_2(^{34}\text{S}) = 0.125$.

considered in the present paper. As expected, at sub-barrier energies the deviation from the UFF is larger in the case of reactions with strongly deformed target nuclei and large factor $Z_1 \times Z_2$ ($^{16}\text{O}, ^{40}\text{Ar}, ^{48}\text{Ca}+^{154}\text{Sm}, ^{74}\text{Ge}+^{74}\text{Ge}$). For the reactions $^{16}\text{O}, ^{40}\text{Ar}+^{144}\text{Sm}$ with spherical targets, the experimental cross sections are rather close to the UFF.

To separate the effects of deformation and neutron transfer, we firstly consider the reactions with deformed nuclei in which the Q value for the neutron transfer is negative (i.e., the neutron transfers can be disregarded). In Figs. 3 and 4, the calculated capture cross sections for the reactions $^{16}\text{O}, ^{48}\text{Ca}, ^{40}\text{Ar}+^{154}\text{Sm}$, and $^{74}\text{Ge}+^{74}\text{Ge}$ are in good agreement with the available experimental data [32,33,35,36] showing that the quadrupole deformations of the interacting nuclei are the main reasons for the enhancement of the capture cross section at sub-barrier energies. The quadrupole deformation parameters β_2 are taken from Ref. [40] for the deformed even-even nuclei. In Ref. [40] the quadrupole deformation parameters β_2 for the first excited 2^+ states of nuclei are given. For the nuclei deformed in the ground state, the β_2 in 2^+ state is similar to the β_2 in the ground state and we use β_2 from Ref. [40] in the calculations. For double magic nuclei, in the ground state we take $\beta_2 = 0$. In Ref. [41] the experimentally observed enhancement of sub-barrier fusion for the reactions $^{16}\text{O}, ^{48}\text{Ca}+^{154}\text{Sm}$, and $^{74}\text{Ge}+^{74}\text{Ge}$ was explained by the nucleon transfer and neck formation effects. However, in the

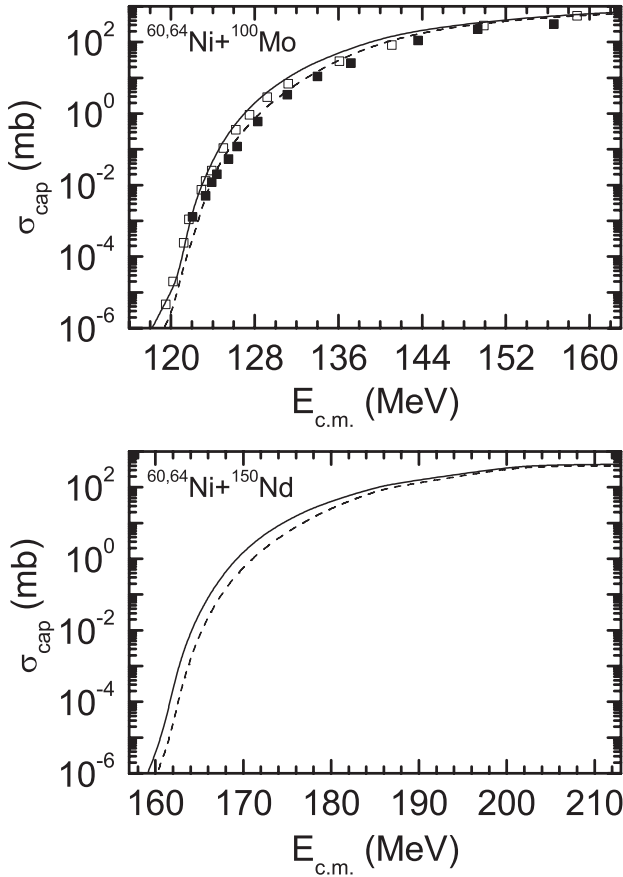


FIG. 9. The same as Fig. 3, for the indicated reactions $^{64}\text{Ni}+^{100}\text{Mo}$, ^{150}Nd (solid lines) and $^{60}\text{Ni}+^{100}\text{Mo}$, ^{150}Nd (dashed lines). The experimental data for the reactions $^{60}\text{Ni}+^{100}\text{Mo}$ (solid squares) and $^{64}\text{Ni}+^{100}\text{Mo}$ (open squares) are from Refs. [11, 49]. The following quadrupole deformation parameters are used: $\beta_2(^{62}\text{Ni}) = 0.1978$ [40], $\beta_2(^{98}\text{Mo}) = 0.1684$ [40], $\beta_2(^{100}\text{Mo}) = 0.2309$ [40], $\beta_2(^{148}\text{Nd}) = 0.2036$ [40], $\beta_2(^{150}\text{Nd}) = 0.2848$ [40], and $\beta_2(^{64}\text{Ni}) = 0.087$.

present article we demonstrate that a good agreement with the experimental data at sub-barrier energies could be reached taking only the quadrupole deformations of interacting nuclei into consideration.

We should mention, that for the sub-barrier energies the results of calculations are very sensitive to the quadrupole deformation parameters β_2 of the interacting nuclei. Because there are uncertainties in the definition of the values of β_2 in light- and medium-mass nuclei, one can extract the quadrupole deformation parameters of these nuclei from the comparison of the calculated capture cross sections with the experimental data. The best case is when the projectile or target is the spherical double magic nucleus and there are no neutron transfer channels with the large positive Q values. In this way by describing the reactions $^{28}\text{Si}+^{90}\text{Zr}$, ^{144}Sm , $^{34}\text{S}+^{168}\text{Er}$, $^{36}\text{S}+^{90,96}\text{Zr}$, $^{40}\text{Ar}+^{112,116,122}\text{Sn}$, ^{144}Sm , $^{58}\text{Ni}+^{58}\text{Ni}$, $^{64}\text{Ni}+^{100}\text{Mo}$, ^{74}Ge (Figs. 5–10), we extract the following values of the quadrupole deformation parameter $\beta_2 = 0.30$, 0.125, 0, 0.25, 0.05, 0.087, 0, 0.08, 0.12, 0.11, 0.1, and 0.05 for the nuclei ^{28}Si , ^{34}S , ^{36}S , ^{40}Ar , ^{58}Ni , ^{64}Ni , ^{90}Zr , ^{96}Zr , ^{112}Sn ,

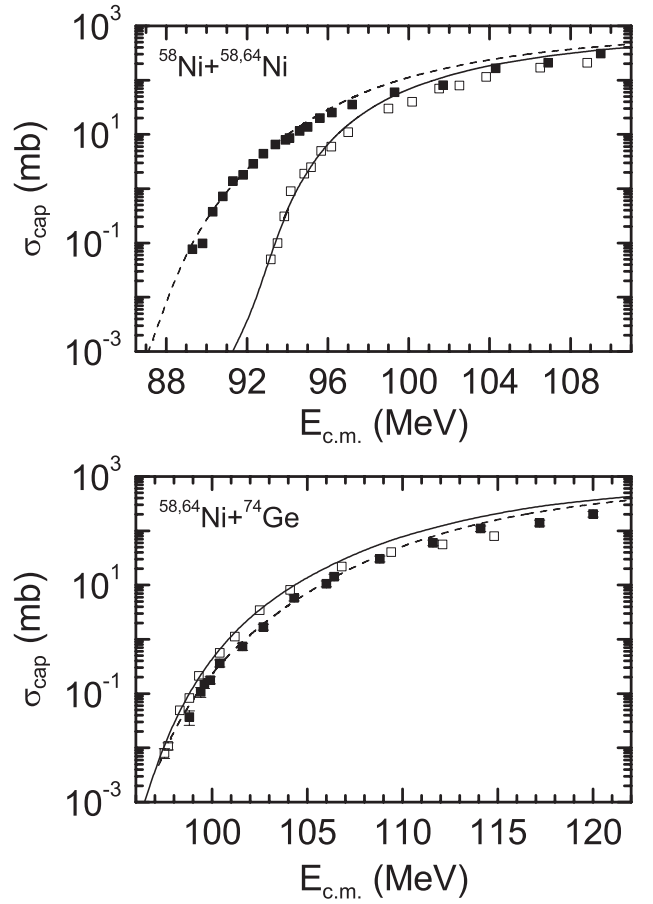


FIG. 10. The same as Fig. 3, for the indicated reactions $^{58}\text{Ni}+^{64}\text{Ni}$, ^{74}Ge (dashed lines) and $^{58}\text{Ni}+^{58}\text{Ni}$, $^{64}\text{Ni}+^{74}\text{Ge}$ (solid lines). The experimental data (symbols) are from Ref. [50]. The following quadrupole deformation parameters are used: $\beta_2(^{60}\text{Ni}) = 0.207$ [40], $\beta_2(^{72}\text{Ge}) = 0.2424$ [40], $\beta_2(^{74}\text{Ge}) = 0.2825$ [40], $\beta_2(^{58}\text{Ni}) = 0.05$, and $\beta_2(^{62}\text{Ni}) \approx \beta_2(^{64}\text{Ni}) = 0.087$ (here, $^{62,64}\text{Ni}$ are in their ground states).

^{116}Sn , ^{122}Sn , and ^{144}Sm , respectively. Note that almost the same values of quadrupole deformation parameters of nuclei in the ground state were predicted within the mean-field and the microscopic-macroscopic models [51]. For the nuclei ^{40}Ar , ^{96}Zr , ^{112}Sn , ^{116}Sn , and ^{122}Sn , the extracted β_2 are equal to the experimental ones from Ref. [40]. These extracted deformation parameters we use in calculations in the next subsection. In our approach, the deformation and statistical effects model the coupling of the relative motion with low-lying collective modes which were explicitly treated in Ref. [23] for the case of almost spherical nuclei.

B. Effect of neutron transfer

Several experiments were performed to understand the effect of neutron transfer in the fusion (capture) reactions. The choice of the projectile-target combination is crucial, and for the systems studied one can make unambiguous statements regarding the neutron transfer process with a positive Q value when the interacting nuclei are double magic or semimagic spherical nuclei. In this case one can disregard the strong nuclear deformation effects before the neutron

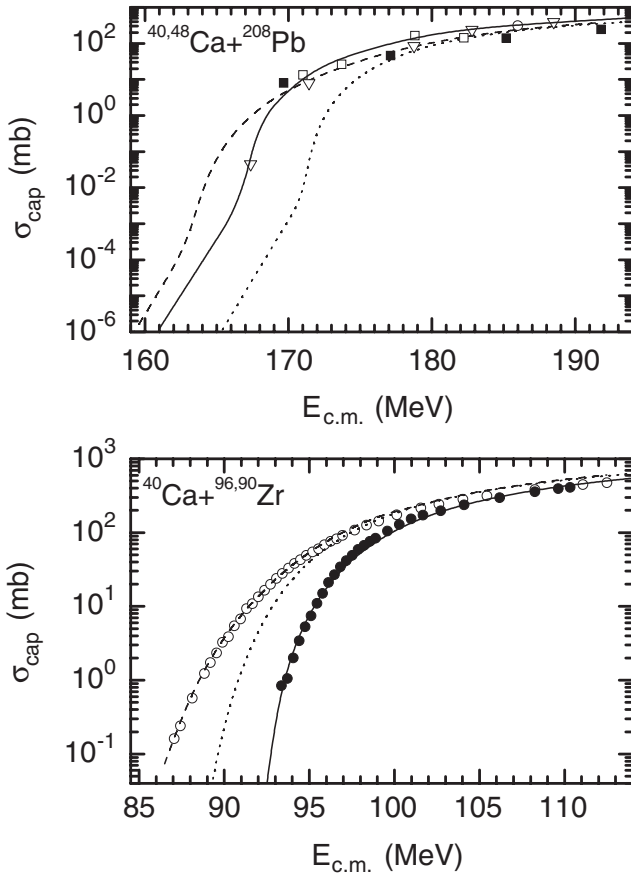


FIG. 11. The same as Fig. 3, for the indicated reactions $^{40}\text{Ca}+^{96}\text{Zr}$, ^{208}Pb (dashed lines), $^{40}\text{Ca}+^{90}\text{Zr}$ (solid line), and $^{48}\text{Ca}+^{208}\text{Pb}$ (solid line and open squares and triangles). For the reactions $^{40}\text{Ca}+^{96}\text{Zr}$, ^{208}Pb , the calculated capture cross sections without taking into consideration the neutron transfer process are shown by dotted lines. The experimental data (symbols) are from Refs. [37–39]. The following quadrupole deformation parameters are used: $\beta_2(^{42}\text{Ca}) = 0.247$ [40], $\beta_2(^{94}\text{Zr}) = 0.09$ [40], $\beta_2(^{96}\text{Zr}) = 0.08$, and $\beta_2(^{40}\text{Ca}) = \beta_2(^{48}\text{Ca}) = \beta_2(^{90}\text{Zr}) = \beta_2(^{206,208}\text{Pb}) = 0$.

transfer. The good examples are the reactions with the spherical nuclei: $^{40}\text{Ca}+^{208}\text{Pb}$ ($Q_{2n} = 5.7$ MeV) and $^{40}\text{Ca}+^{96}\text{Zr}$ ($Q_{2n} = 5.5$ MeV). In Fig. 2 (lower part), one can see that the reduced capture cross sections in these reactions strongly deviate from the UFF in contrast to those in the reactions $^{48}\text{Ca}+^{208}\text{Pb}$ and $^{48}\text{Ca}+^{96}\text{Zr}$, where the neutron transfer channels are suppressed (the negative Q values). Because the transfer of protons is shielded by the Coulomb barrier, it occurs when two nuclei almost touch each other [30] (i.e., after a capture). Thus, the proton transfer can be disregarded in the calculations of capture cross sections.

Following the hypothesis of Ref. [10], we assume that the sub-barrier capture mainly depends on the two-neutron transfer with the positive Q value. Our assumption is that, before the projectile is captured by the target nucleus (before the crossing of the Coulomb barrier) which is the slow process, the two-neutron transfer occurs at larger separations that can lead to the population of the first 2^+ state in the recipient nucleus [52]. Because after two-neutron transfer,

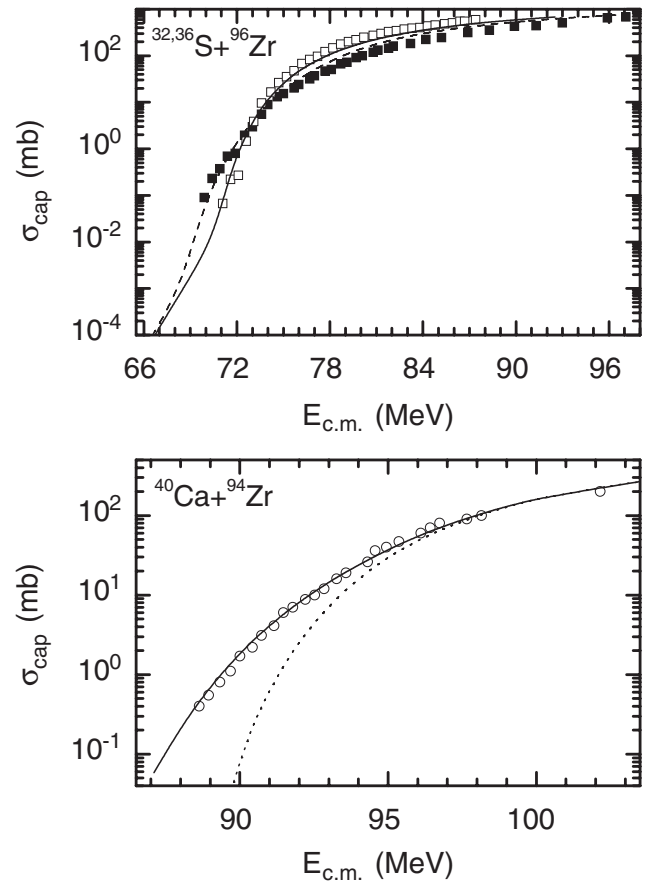


FIG. 12. The same as Fig. 3, for the indicated reactions $^{40}\text{Ca}+^{94}\text{Zr}$ (solid line), $^{32}\text{S}+^{96}\text{Zr}$ (dashed line and solid squares), and $^{36}\text{S}+^{96}\text{Zr}$ (solid line and open squares). For the $^{40}\text{Ca}+^{94}\text{Zr}$ reaction, the calculated capture cross sections without taking into consideration the neutron transfer process are shown by dotted line. The experimental data (symbols) are from Refs. [45,46,53]. The following quadrupole deformation parameters are used: $\beta_2(^{42}\text{Ca}) = 0.247$ [40], $\beta_2(^{94}\text{Zr}) = 0.09$ [40], $\beta_2(^{92}\text{Zr}) = 0.1028$ [40], $\beta_2(^{96}\text{Zr}) = 0.08$, and $\beta_2(^{36}\text{S}) = \beta_2(^{40}\text{Ca}) = 0$.

the mass numbers, the deformation parameters of interacting nuclei, and, respectively, the height and shape of the Coulomb barrier are changed, one can expect the enhancement or suppression of the capture. For example, after the neutron transfer in the reaction $^{40}\text{Ca}(\beta_2 = 0) + ^{208}\text{Pb}(\beta_2 = 0) \rightarrow ^{42}\text{Ca}(\beta_2 = 0.247) + ^{206}\text{Pb}(\beta_2 = 0)$ ($^{40}\text{Ca}(\beta_2 = 0) + ^{96}\text{Zr}(\beta_2 = 0.08) \rightarrow ^{42}\text{Ca}(\beta_2 = 0.247) + ^{94}\text{Zr}(\beta_2 = 0.09)$) the deformation of the nuclei increases and the mass asymmetry of the system decreases, and, thus, the value of the Coulomb barrier decreases and the capture cross section becomes larger (Fig. 11). We observe the same behavior in the reactions $^{64}\text{Ni}+^{132}\text{Sn}$ (Fig. 8) $^{58}\text{Ni}+^{64}\text{Ni}$, ^{74}Ge (Fig. 10), $^{32}\text{S}+^{96}\text{Zr}$, $^{40}\text{Ca}+^{94}\text{Zr}$ (Fig. 12), $^{40}\text{Ca}+^{192}\text{Os}$, ^{198}Pt (Fig. 13), and $^{40}\text{Ca}+^{48}\text{Ca}$, $^{116,124}\text{Sn}$ (Fig. 14). One can see a good agreement between the calculated results and the experimental data. For some reactions at energies above the Coulomb barrier, the small deviation between the calculated results and experimental data probably arises from the fact that the fusion-fission and quasifission channels [58,59] were not taken into consideration in the experimental

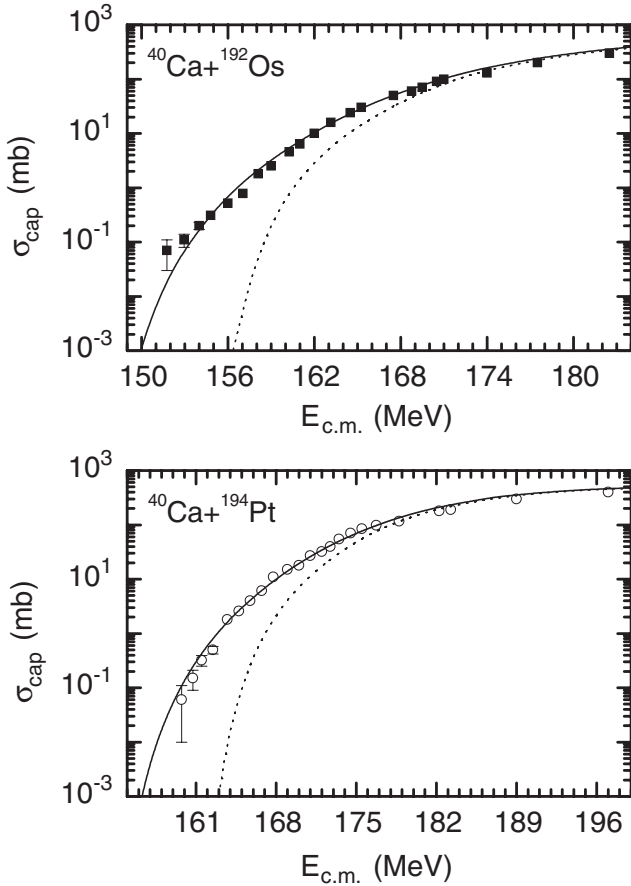


FIG. 13. The same as Fig. 3, for the indicated reactions $^{40}\text{Ca}+^{192}\text{Os}$, ^{194}Pt (solid lines). The calculated capture cross sections without taking into consideration the neutron transfer process are shown by dotted lines. The experimental data (symbols) are from Ref. [54]. The following quadrupole deformation parameters are used: $\beta_2(^{42}\text{Ca})=0.247$ [40], $\beta_2(^{192}\text{Os})=0.1667$ [40], $\beta_2(^{190}\text{Os})=0.1775$ [40], $\beta_2(^{194}\text{Pt})=0.1426$ [40], $\beta_2(^{192}\text{Pt})=0.1532$ [40], and $\beta_2(^{40}\text{Ca})=0$.

capture cross sections. So, our results show that the observed capture enhancement at sub-barrier energies for the reactions mentioned above is related to the two-neutron transfer channel. For these reactions, there is a large deflection from the UFF (see lower part of Fig. 2). Note that the strong population of the yrast states, and in particular of the first 2^+ state of even Ar (Ca) isotopes via the neutron pick-up channels in the $^{40}\text{Ar}+^{208}\text{Pb}$ ($^{40}\text{Ca}+^{96}\text{Zr}$) reaction was experimentally found in Ref. [52]. In the calculations, for such excited recipient nuclei we use the experimental deformation parameters β_2 related to the first 2^+ states from the table of Ref. [40]. We assume that after two-neutron transfer the residues of donor nuclei remain in the ground state with corresponding quadrupole deformation.

One can find the reactions with positive two-neutron transfer Q values where the transfer weakly influences or even suppresses the capture process. This happens if after transfer the deformations of nuclei almost do not change or even decrease. For instance, in the reactions $^{32}\text{S}(\beta_2=0.312)+^{96}\text{Zr}(\beta_2=0.08) \rightarrow ^{34}\text{S}(\beta_2=0.252) + ^{94}\text{Zr}(\beta_2=$

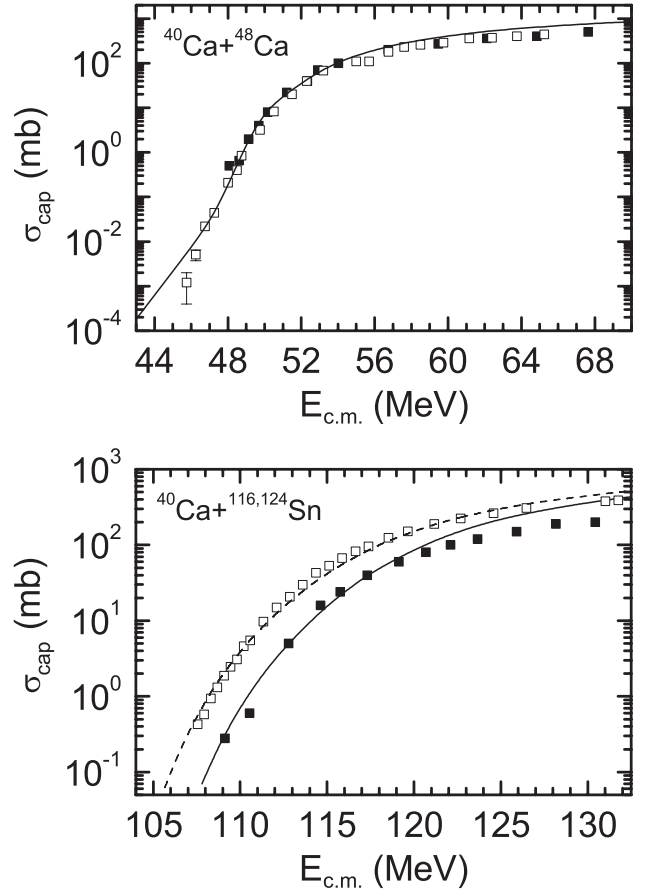


FIG. 14. The same as Fig. 3, for the indicated reactions $^{40}\text{Ca}+^{48}\text{Ca}$, ^{116}Sn (solid lines), and $^{40}\text{Ca}+^{124}\text{Sn}$ (dashed line). The experimental data (symbols) are from Refs. [55–57]. The following quadrupole deformation parameters are used: $\beta_2(^{42}\text{Ca})=0.247$ [40], $\beta_2(^{116}\text{Sn})=0.1118$ [40], $\beta_2(^{122}\text{Sn})=0.1036$ [40], and $\beta_2(^{46}\text{Ca})=\beta_2(^{40}\text{Ca})=0$.

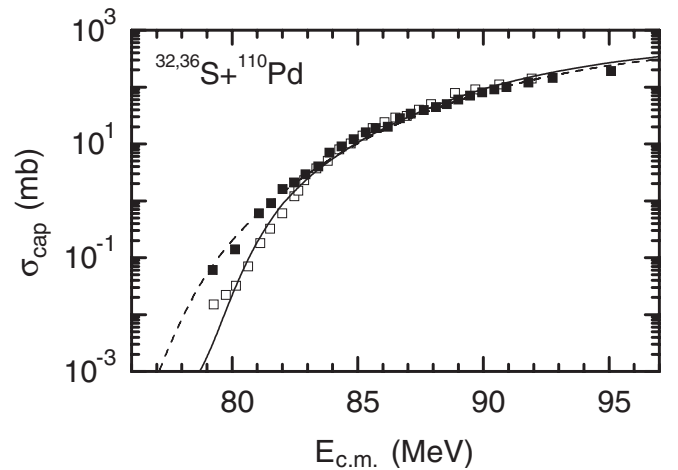


FIG. 15. The same as Fig. 3, for the indicated reactions $^{32}\text{S}+^{110}\text{Pd}$ (dashed line and solid squares) and $^{36}\text{S}+^{110}\text{Pd}$ (solid line and open squares). The experimental data (symbols) are from Ref. [8]. The following quadrupole deformation parameters are used: $\beta_2(^{34}\text{S})=0.252$ [40], $\beta_2(^{108}\text{Pd})=0.243$ [40], $\beta_2(^{110}\text{Pd})=0.257$ [40], and $\beta_2(^{36}\text{S})=0$.

0.09), $^{60}\text{Ni}(0.05 < \beta_2 \leq 0.1) + ^{100}\text{Mo}(\beta_2 = 0.231) \rightarrow ^{62}\text{Ni}(\beta_2 = 0.198) + ^{98}\text{Mo}(\beta_2 = 0.168)$, and $^{60}\text{Ni}(0.05 < \beta_2 \leq 0.1) + ^{150}\text{Nd}(\beta_2 = 0.285) \rightarrow ^{62}\text{Ni}(\beta_2 = 0.198) + ^{148}\text{Nd}(\beta_2 = 0.204)$ one can expect weak dependence of the capture cross section on the neutron transfer (Figs. 9 and 12). There is the experimental indication of such an effect for the $^{60}\text{Ni} + ^{100}\text{Mo}$ reaction [11]. The weak influence of neutron transfer on the capture process is also found in the reactions $^{32}\text{S} + ^{110}\text{Pd}$, ^{154}Sm , ^{208}Pb (Figs. 15 and 16), $^{28}\text{Si} + ^{94}\text{Zr}$, ^{142}Ce , ^{154}Sm , ^{208}Pb (Figs. 5 and 17). The same behavior is expected in the reactions $^{84}\text{Kr} + ^{138}\text{Ce}$, ^{140}Nd .

Note that our model predicts almost the same capture cross sections for the reactions with positive Q values ^6He , ^9Li , $^{11}\text{Be} + ^{206}\text{Pb}$, $^{18}\text{O} + ^{58}\text{Ni}$ and for the reactions without neutron transfer ^4He , ^7Li , $^9\text{Be} + ^{208}\text{Pb}$, $^{16}\text{O} + ^{60}\text{Ni}$, respectively. Here, the break-up channels are not taken into consideration in the calculations.

In Fig. 18, the capture cross sections for the reactions $^{58,64}\text{Ni} + ^{207}\text{Pb}$ are predicted. As seen, there is considerable difference between the capture cross sections in these two reactions because of the existence of the two-neutron transfer channel ($Q_{2n} = 5.6$ MeV) in the reaction $^{58}\text{Ni} + ^{207}\text{Pb} \rightarrow$

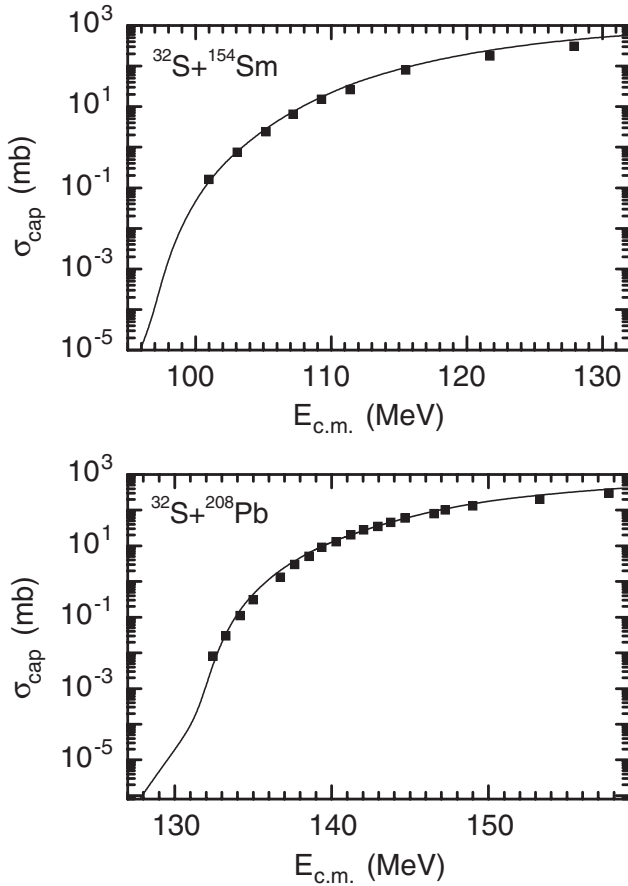


FIG. 16. The same as Fig. 3, for the indicated reactions $^{32}\text{S} + ^{154}\text{Sm}$, ^{208}Pb . The experimental data (symbols) are from Refs. [60,61]. The following quadrupole deformation parameters are used: $\beta_2(^{34}\text{S}) = 0.252$ [40], $\beta_2(^{152}\text{Sm}) = 0.3064$ [40], and $\beta_2(^{206}\text{Pb}) = 0$.

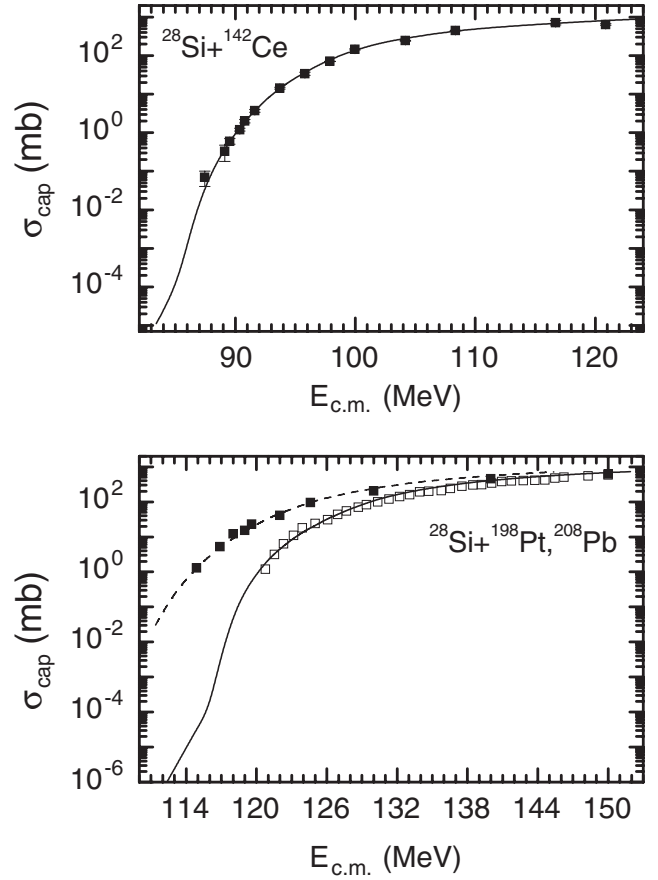


FIG. 17. The same as Fig. 3, for the indicated reactions $^{28}\text{Si} + ^{142}\text{Ce}$, ^{208}Pb (solid lines), and $^{28}\text{Si} + ^{198}\text{Pt}$ (dashed line). The experimental data (symbols) are from Refs. [62–64]. The following quadrupole deformation parameters are used: $\beta_2(^{30}\text{Si}) = 0.315$ [40], $\beta_2(^{140}\text{Ce}) = 0.1012$ [40], $\beta_2(^{196}\text{Pt}) = 0.1296$ [40], and $\beta_2(^{206}\text{Pb}) = 0$.

$^{60}\text{Ni} + ^{205}\text{Pb}$. Thus, the study of these reactions could be a good test for the conclusion about the effect of neutron transfer. It will be interesting to compare the role of the neutron transfer channel in the reactions with spherical nuclei mentioned above (Fig. 11) and with deformed targets, $^{40}\text{Ca} + ^{154}\text{Sm}$, ^{238}U (Fig. 19). Because of a change of the regime of interaction (the turning off of the nuclear forces and friction) at sub-barrier energies [18–20], the curve related to the capture cross section as a function of bombarding energy has smaller slope (see Figs. 3–9, 11, 12 and 14–17). This effect is more visible in the capture of spherical nuclei without the neutron transfer. However, the present experimental data on the capture process at strongly sub-barrier energies are rather poor.

V. ORIGIN OF FUSION HINDRANCE IN REACTIONS WITH MEDIUM-MASS NUCLEI AT DEEP SUB-BARRIER ENERGIES

Because the sum of the fusion cross section σ_{fus} and the quasifission cross section σ_{qf} gives the capture cross section,

$$\sigma_{\text{cap}} = \sigma_{\text{fus}} + \sigma_{\text{qf}},$$

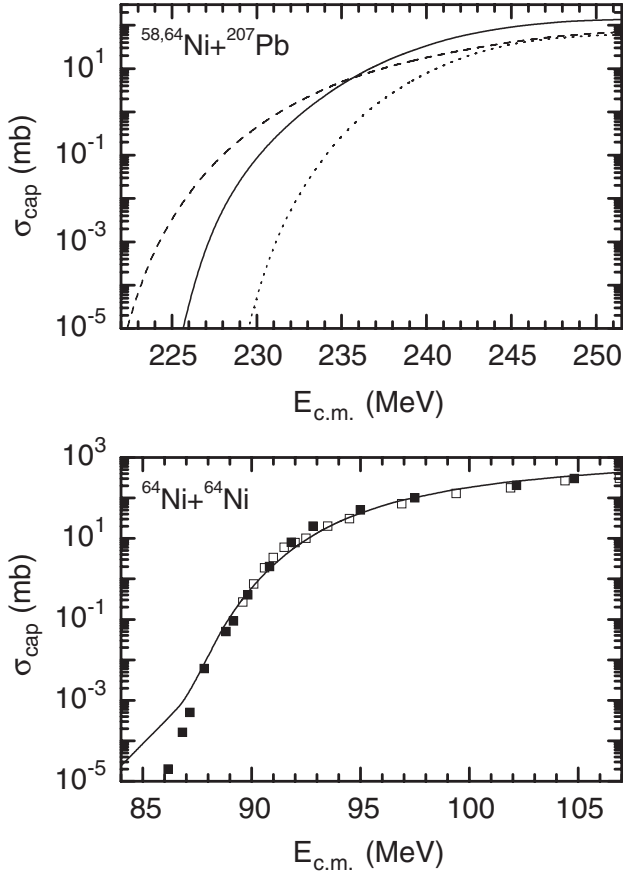


FIG. 18. The same as Fig. 3, for the indicated reactions $^{58}\text{Ni}+^{207}\text{Pb}$ (dashed line), $^{64}\text{Ni}+^{64}\text{Ni}$ (solid line), and $^{64}\text{Ni}+^{207}\text{Pb}$ (solid line). For the $^{58}\text{Ni}+^{207}\text{Pb}$ reaction, the calculated capture cross sections without taking into consideration the neutron transfer process are shown by dotted line. The experimental data (symbols) are from Refs. [50,66]. The following quadrupole deformation parameters are used: $\beta_2(^{60}\text{Ni})=0.207$ [40], $\beta_2(^{58}\text{Ni})=0.05$, $\beta_2(^{64}\text{Ni})=0.087$, and $\beta_2(^{205,207}\text{Pb})=0$.

one can estimate the relative contributions of σ_{fus} and σ_{qf} to σ_{cap} . In Figs. 14, 18, and 20 the calculated capture cross section are presented for the reactions $^{40}\text{Ca}+^{48}\text{Ca}$, $^{64}\text{Ni}+^{64}\text{Ni}$, and $^{36}\text{S}+^{48}\text{Ca}$, ^{64}Ni . As seen, at energies above and just below the Coulomb barriers $\sigma_{\text{cap}} = \sigma_{\text{fus}}$. The difference between the sub-barrier capture and fusion cross sections becomes larger with decreasing bombarding energy $E_{\text{c.m.}}$. One can see the same effect for the $^{16}\text{O}+^{208}\text{Pb}$ reaction [18]. Assuming that the estimated capture and the measured fusion cross sections are correct, the small fusion cross section at energies well below the Coulomb barrier may indicate that another reaction channel is preferable and the system goes to this channel after the capture. The observed hindrance factor may be understood in terms of quasifission whose cross section should be added to the σ_{fus} to obtain a meaningful comparison with the calculated capture cross section.

At deep sub-barrier energies, the quasifission event corresponds to the formation of a nuclear-molecular state or dinuclear system with small excitation energy that separates (in competition with the compound nucleus formation process) by

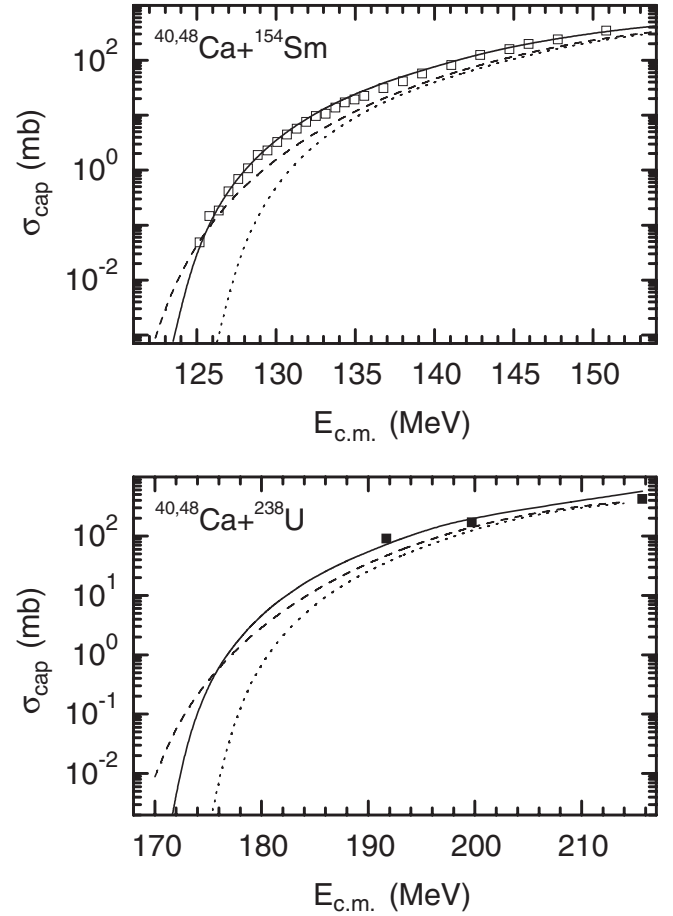


FIG. 19. The same as Fig. 3, for the indicated reactions $^{40}\text{Ca}+^{154}\text{Sm}$, ^{238}U (dashed lines), and $^{48}\text{Ca}+^{154}\text{Sm}$, ^{238}U (solid lines). For the reactions $^{40}\text{Ca}+^{154}\text{Sm}$, ^{238}U , the calculated capture cross sections without taking into consideration the neutron transfer process are shown by dotted line. The experimental data (symbols) for the reactions $^{48}\text{Ca}+^{154}\text{Sm}$, ^{238}U are from Refs. [32,65]. The following quadrupole deformation parameters are used: $\beta_2(^{42}\text{Ca})=0.247$ [40], $\beta_2(^{152}\text{Sm})=0.3055$ [40], $\beta_2(^{154}\text{Sm})=0.341$ [40], $\beta_2(^{236}\text{U})=0.2821$ [40], $\beta_2(^{238}\text{U})=0.2863$ [40], and $\beta_2(^{48}\text{Ca})=0$.

the quantum tunneling through the Coulomb barrier in a binary event with mass and charge close to the entrance channel. In this sense the quasifission is the general phenomenon which takes place in the reactions with the massive [14–17], medium-mass, and, probably, light nuclei. For the medium-mass and light nuclei, this reaction channel is expected to be at deep sub-barrier energies and has to be studied in future experiments: From the measurement of the mass (charge) distribution in the collisions with total momentum transfer one can show the distinct components from the quasifission. Because of these energies, the angular momentum $J < 10$ and the angular distribution would have small anisotropy. The low-energy experimental data would probably provide straight information because the high-energy data may be shaded by competing nucleon transfer processes. Note that the binary decay events were already observed experimentally in Ref. [69] for the $^{58}\text{Ni}+^{124}\text{Sn}$ reaction at energies below the Coulomb barrier

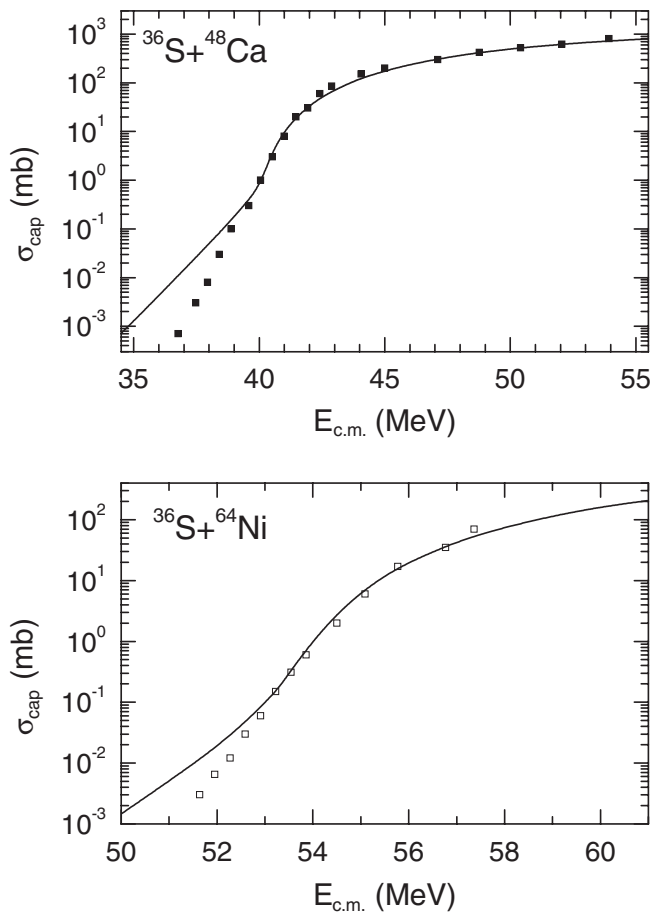


FIG. 20. The same as Fig. 3, for the indicated reactions $^{36}\text{S}+^{48}\text{Ca}$, ^{64}Ni . The experimental data (symbols) are from Refs. [67, 68]. The following quadrupole deformation parameters are used: $\beta_2(^{64}\text{Ni}) = 0.087$ and $\beta_2(^{36}\text{S}) = \beta_2(^{48}\text{Ca}) = 0$.

but assumed to be related to deep-inelastic scattering. At energies above the Coulomb barrier the hindrance to fusion

was revealed in Ref. [70] for the reactions $^{58}\text{Ni}+^{124}\text{Sn}$ and $^{16}\text{O}+^{208}\text{Pb}$.

VI. SUMMARY

The quantum diffusion approach was applied to study the capture process in the reactions with deformed and spherical nuclei at sub-barrier energies. The available experimental data at energies above and below the Coulomb barrier are well described. As shown, the experimentally observed sub-barrier fusion enhancement is mainly related to the quadrupole deformation of the colliding nuclei and neutron transfer with the positive Q value. The change of the magnitude of the capture cross section after the neutron transfer occurs because of the change of the deformations of nuclei. When after the neutron transfer the deformations of nuclei do not change or decrease, the neutron transfer weakly influences or suppresses the capture process. It would be interesting to study such types of reactions.

The importance of quasifission near the entrance channel was noticed for the reactions with medium-mass nuclei at extreme sub-barrier energies. The quasifission can explain the difference between the capture and fusion cross sections. One can try to check experimentally these predictions.

ACKNOWLEDGMENTS

We thank H. Jia, D. Lacroix, J.-Q. Li, C. J. Lin, and S.-G. Zhou for fruitful discussions and suggestions. This work was supported by Deutsche Forschungsgemeinschaft, National Natural Science Foundation of China, and Russian Foundation for Basic Research. The IN2P3(France)–JINR(Dubna), MTA(Hungary)–JINR(Dubna), and Polish–JINR(Dubna) Cooperation Programmes are gratefully acknowledged.

- [1] A. B. Balantekin and N. Takigawa, *Rev. Mod. Phys.* **70**, 77 (1998).
- [2] L. F. Canto, P. R. S. Gomes, R. Donangelo, and M. S. Hussein, *Phys. Rep.* **424**, 1 (2006).
- [3] C. A. Bertulani, *EPJ Web Conf.* **17**, 15001 (2011).
- [4] W. Henning, F. L. H. Wolfs, J. P. Schiffer, and K. E. Rehm, *Phys. Rev. Lett.* **58**, 318 (1987).
- [5] P. H. Stelson, H. J. Kim, M. Beckerman, D. Shapira, and R. L. Robinson, *Phys. Rev. C* **41**, 1584 (1990); C. L. Jiang, K. E. Rehm, J. Gehring, B. Glagola, W. Kutschera, M. Rhein, and A. H. Wuosmaa, *Phys. Lett. B* **337**, 59 (1994).
- [6] R. Pengo *et al.*, *Nucl. Phys. A* **411**, 255 (1983).
- [7] R. B. Roberts *et al.*, *Phys. Rev. C* **47**, R1831 (1993); D. Ackermann *et al.*, *Nucl. Phys. A* **609**, 91 (1996).
- [8] A. M. Stefanini, D. Ackermann, L. Corradi, J. H. He, G. Montagnoli, S. Beghini, F. Scarlassara, and G. F. Segato, *Phys. Rev. C* **52**, R1727 (1995).
- [9] A. A. Sonzogni, J. D. Bierman, M. P. Kelly, J. P. Lestone, J. F. Liang, and R. Vandenbosch, *Phys. Rev. C* **57**, 722 (1998).
- [10] R. A. Broglia, C. H. Dasso, S. Landowne, and A. Winther, *Phys. Rev. C* **27**, 2433 (1983); R. A. Broglia, C. H. Dasso, S. Landowne, and G. Pollarolo, *Phys. Lett. B* **133**, 34 (1983).
- [11] F. Scarlassara *et al.*, *EPJ Web Conf.* **17**, 05002 (2011).
- [12] C. L. Jiang *et al.*, *Phys. Rev. Lett.* **89**, 052701 (2002).
- [13] K. Langanke and C. A. Barnes, *Adv. Nucl. Phys.* **22**, 173 (1996); A. Aprahamian, K. Langanke, and M. Wiescher, *Prog. Part. Nucl. Phys.* **54**, 535 (2005).
- [14] J. G. Keller *et al.*, *Nucl. Phys. A* **452**, 173 (1986).
- [15] V. V. Volkov, *Part. Nucl.* **35**, 797 (2004).
- [16] G. G. Adamian, N. V. Antonenko, and W. Scheid, *Phys. Rev. C* **68**, 034601 (2003); in *Lecture Notes in Physics 848, Clusters in Nuclei*, Vol. 2, edited by C. Beck (Springer-Verlag, Berlin, 2012), p. 165.
- [17] G. Giardina *et al.*, *Nucl. Phys. A* **671**, 165 (2000); A. Nasirov *et al.*, *ibid.* **759**, 342 (2005); Z.-Q. Feng, G.-M. Jin, J.-Q. Li, and W. Scheid, *Phys. Rev. C* **76**, 044606 (2007); H. Q. Zhang, C. L. Zhang, C. J. Lin, Z. H. Liu, F. Yang, A. K. Nasirov, G. Mandaglio, M. Manganaro, and G. Giardina, *ibid.* **81**, 034611 (2010).

- [18] V. V. Sargsyan, G. G. Adamian, N. V. Antonenko, and W. Scheid, *Eur. Phys. J. A* **45**, 125 (2010).
- [19] V. V. Sargsyan, G. G. Adamian, N. V. Antonenko, W. Scheid, and H. Q. Zhang, *Eur. Phys. J. A* **47**, 38 (2011).
- [20] V. V. Sargsyan, G. G. Adamian, N. V. Antonenko, W. Scheid, and H. Q. Zhang, *J. Phys.: Conf. Ser.* **282**, 012001 (2011); *EPJ Web Conf.* **17**, 04003 (2011).
- [21] A. S. Zubov, V. V. Sargsyan, G. G. Adamian, and N. V. Antonenko, *Phys. Rev. C* **84**, 044320 (2011).
- [22] A. S. Zubov, V. V. Sargsyan, G. G. Adamian, N. V. Antonenko, and W. Scheid, *Phys. Rev. C* **81**, 024607 (2010); **82**, 034610 (2010).
- [23] S. Ayik, B. Yilmaz, and D. Lacroix, *Phys. Rev. C* **81**, 034605 (2010).
- [24] V. V. Sargsyan, Z. Kanokov, G. G. Adamian, N. V. Antonenko, and W. Scheid, *Phys. Rev. C* **80**, 034606 (2009); **80**, 047603 (2009); V. V. Sargsyan, Z. Kanokov, G. G. Adamian, and N. V. Antonenko, *Part. Nucl.* **41**, 175 (2010).
- [25] G. G. Adamian, N. V. Antonenko, Z. Kanokov, and V. V. Sargsyan, *Teor. Mat. Fiz.* **145**, 87 (2005); *Theor. Math. Phys.* **145**, 1443 (2006); Z. Kanokov, Yu. V. Palchikov, G. G. Adamian, N. V. Antonenko, and W. Scheid, *Phys. Rev. E* **71**, 016121 (2005); Yu. V. Palchikov, Z. Kanokov, G. G. Adamian, N. V. Antonenko, and W. Scheid, *ibid.* **71**, 016122 (2005); R. A. Kuz'yakin, V. V. Sargsyan, G. G. Adamian, and N. V. Antonenko, *Phys. Rev. A* **83**, 062117 (2011); **84**, 032117 (2011).
- [26] H. Hofmann, *Phys. Rep.* **284**, 137 (1997); C. Rummel and H. Hofmann, *Nucl. Phys. A* **727**, 24 (2003).
- [27] N. Takigawa, S. Ayik, K. Washiyama, and S. Kimura, *Phys. Rev. C* **69**, 054605 (2004); S. Ayik, B. Yilmaz, A. Gokalp, O. Yilmaz, and N. Takigawa, *ibid.* **71**, 054611 (2005).
- [28] G. Hupin and D. Lacroix, *Phys. Rev. C* **81**, 014609 (2010).
- [29] V. V. Dodonov and V. I. Man'ko, *Trudy Fiz. Inst. AN* **167**, 7 (1986).
- [30] G. G. Adamian, A. K. Nasirov, N. V. Antonenko, and R. V. Jolos, *Phys. Part. Nucl.* **25**, 583 (1994).
- [31] K. Washiyama, D. Lacroix, and S. Ayik, *Phys. Rev. C* **79**, 024609 (2009); S. Ayik, K. Washiyama, and D. Lacroix, *ibid.* **79**, 054606 (2009).
- [32] G. N. Knyazheva *et al.*, *Phys. Rev. C* **75**, 064602 (2007); A. M. Stefanini *et al.*, *Eur. Phys. J. A* **23**, 473 (2005).
- [33] J. R. Leigh *et al.*, *Phys. Rev. C* **52**, 3151 (1995).
- [34] D. E. DiGregorio *et al.*, *Phys. Rev. C* **39**, 516 (1989).
- [35] M. Beckerman, M. K. Salomaa, J. Wiggins, and R. Rohe, *Phys. Rev. C* **28**, 1963 (1983).
- [36] W. Reisdorf *et al.*, *Nucl. Phys. A* **438**, 212 (1985).
- [37] H. Timmers *et al.*, *Nucl. Phys. A* **633**, 421 (1998).
- [38] A. J. Pacheco *et al.*, *Phys. Rev. C* **45**, 2861 (1992); R. Bock *et al.*, *Nucl. Phys. A* **388**, 334 (1982).
- [39] E. Prokhorova *et al.*, *Nucl. Phys. A* **802**, 45 (2008).
- [40] S. Raman, C. W. Nestor Jr., and P. Tikkanen, *At. Data Nucl. Data Tables* **78**, 1 (2001).
- [41] J. M. B. Shorto, P. R. S. Gomes, J. Lubian, L. F. Canto, and P. Lotti, *Phys. Rev. C* **81**, 044601 (2010).
- [42] S. Kalkal *et al.*, *Phys. Rev. C* **81**, 044610 (2010).
- [43] S. Gil *et al.*, *Phys. Rev. Lett.* **65**, 3100 (1990).
- [44] G. P. A. Nobre, L. C. Chamon, L. R. Gasques, B. V. Carlson, and I. J. Thompson, *Phys. Rev. C* **75**, 044606 (2007).
- [45] H. Q. Zhang *et al.*, *Phys. Rev. C* **82**, 054609 (2010).
- [46] A. M. Stefanini *et al.*, *Phys. Rev. C* **62**, 014601 (2000).
- [47] C. R. Morton, A. C. Berriman, R. D. Butt, M. Dasgupta, A. Godley, D. J. Hinde, and J. O. Newton, *Phys. Rev. C* **62**, 024607 (2000).
- [48] J. F. Liang, D. Shapira, C. J. Gross, R. L. Varner, J. R. Beene, P. E. Mueller, and D. W. Stracener, *Phys. Rev. C* **78**, 047601 (2008).
- [49] C. L. Jiang *et al.*, *Phys. Rev. C* **71**, 044613 (2005).
- [50] M. Beckerman, M. Salomaa, A. Sperduto, J. D. Molitoris, and A. DiRienzo, *Phys. Rev. C* **25**, 837 (1982).
- [51] P. Möller *et al.*, *At. Data Nucl. Data Tables* **59**, 185 (1995).
- [52] S. Szilner *et al.*, *Phys. Rev. C* **76**, 024604 (2007); L. Corradi, G. Pollarolo, and S. Szilner, *J. Phys. G* **36**, 113101 (2009); S. Szilner *et al.*, *J. Phys.: Conf. Ser.* **282**, 012021 (2011); *EPJ Web Conf.* **17**, 03005 (2011); *Phys. Rev. C* **84**, 014325 (2011); L. Corradi *et al.*, *EPJ Web Conf.* **17**, 08004 (2011); *Phys. Rev. C* **84**, 034603 (2011).
- [53] A. M. Stefanini *et al.*, *Phys. Rev. C* **76**, 014610 (2007).
- [54] J. D. Bierman, P. Chan, J. F. Liang, M. P. Kelly, A. A. Sonzogni, and R. Vandenbosch, *Phys. Rev. C* **54**, 3068 (1996).
- [55] H. A. Aljuwair *et al.*, *Phys. Rev. C* **30**, 1223 (1984).
- [56] C. L. Jiang *et al.*, *Phys. Rev. C* **82**, 041601(R) (2010).
- [57] A. M. Stefanini *et al.*, *Eur. Phys. J. A* **23**, 1401 (1997); F. Scarlassara *et al.*, *Nucl. Phys. A* **672**, 99 (2000).
- [58] L. G. Moretto and G. J. Wozniak, *Prog. Part. Nucl. Phys.* **21**, 401 (1988).
- [59] G. Ademard *et al.*, *Phys. Rev. C* **83**, 054619 (2011); *EPJ Web Conf.* **17**, 10005 (2011); Sh. A. Kalandarov, G. G. Adamian, N. V. Antonenko, and W. Scheid, *Phys. Rev. C* **82**, 044603 (2010); **83**, 054611 (2011).
- [60] P. R. S. Gomes *et al.*, *Phys. Rev. C* **49**, 245 (1994).
- [61] M. Dasgupta and D. J. Hinde, *Nucl. Phys. A* **734**, 148 (2004).
- [62] S. Gil *et al.*, *Phys. Rev. C* **51**, 1336 (1995).
- [63] K. Nishio, H. Ikezoe, S. Mitsuoka, and J. Lu, *Phys. Rev. C* **62**, 014602 (2000).
- [64] D. J. Hinde *et al.*, *Nucl. Phys. A* **592**, 271 (1995).
- [65] W. Q. Shen *et al.*, *Phys. Rev. C* **36**, 115 (1987).
- [66] C. L. Jiang *et al.*, *Phys. Rev. Lett.* **93**, 012701 (2004).
- [67] A. M. Stefanini *et al.*, *Phys. Rev. C* **78**, 044607 (2008).
- [68] G. Montagnoli *et al.*, *Nucl. Phys. A* **834**, 159c (2010); *Phys. Rev. C* **82**, 064609 (2010).
- [69] F. L. H. Wolfs, W. Henning, K. E. Rehm, and J. P. Schiffer, *Phys. Lett. B* **196**, 113 (1987).
- [70] G. Pollarolo, *Nucl. Phys. A* **787**, 206c (2007).